

Article

An Analytical Method for Generating Determined Torque Ripple in Synchronous Machine with Interior Magnets by Harmonic Current Injection

Matthias Vollat * , Junchao Li and Frank Gauterin

Institute of Vehicle System Technology, Karlsruher Institut of Technology, 76131 Karlsruhe, Germany; timlijc21@gmail.com (J.L.); frank.gauterin@kit.edu (F.G.)

* Correspondence: Matthias.vollat@kit.edu

Received: 21 September 2020; Accepted: 13 October 2020; Published: 15 October 2020



Abstract: In this paper, we present an extension for an analytical method of calculating the required amplitudes and phase angles of the injected harmonic currents, to generate a determined torque ripple for synchronous machines. With the consideration of reluctance torque in the system equations, this method is valid not only for synchronous machines with surface magnets, but also for those with interior magnets. First, we describe the machine equations as a function of the phase current and the back electromotive force. We then introduce an analytical way to calculate the reluctance torque. After combining the equations, we establish a linear system of equations. The solution of the equation system yields the amplitudes and phase angles of the harmonic currents to be injected. Finally, we validate the equations for calculating the reluctance Torque and the method to generate the determined torque ripple with several finite element method simulations. This allowed us to generate the desired torque fluctuations even for synchronous machines with interior magnets.

Keywords: harmonic current injection; permanent magnet synchronous machines; interior magnets; analytical method; torque ripple

1. Introduction

Thanks to their high power density and low maintenance requirements, permanent magnet synchronous machines (PMSMs) match the requirements for electric traction machines (ETM) in hybrid electric vehicles (HEV) and full electric vehicles (EV) very well [1–3]. Additionally, developments in converter technology have greatly simplified their use in recent years [4,5].

PMSMs do not produce completely constant torque. Even in a steady state, torque fluctuations are generated, which can be a major reason for speed fluctuations. These variations can generate vibrations that cause the entire rest of the system to oscillate. The result can be high noise generation and strong surface vibrations. For many applications of PMSMs, such negative emissions are unacceptable [6].

To reduce these torque fluctuations, many methods have been developed and tested in recent years. Most of these methods use design features on the rotor or stator, and thus change the construction of the machine. There are many examples in the literature, including the distribution of the winding [7,8], an odd number of slots for the stator [9], using single-layer winding or double-layer winding [10], adjusting the magnetic pole and anchor-slot design [11], and other methods to improve the rotor or stator design [12–18]. Although most of the methods provide good results, most of them have to be applied in the conception phase of PMSMs, and are limited to the reduction of the cogging torque.

As an alternative (or supplement) to design features, control-engineering interventions can also bring a reduction in torque oscillations. A prominent representative of control interventions is the harmonic current injection (HCI). Higher harmonic currents are added to the fundamental wave of the current, which reduces the fluctuations in torque of the ETM [19–23].

All the methods mentioned above try to minimize the torque ripple as much as possible. The primary goal should of course be an ETM without torque ripple to reduce noise and vibration emissions. In most cases, however, the electric powertrain of an HEV or EV is made up of more than just the ETM. Therefore, it may also be necessary to create a certain torque ripple on the output end of the ETM. This can reduce vibrations from other sources by excitation in the antiphase. Alternatively, the torque ripple can be used to mimic the low-frequency noise spectrum of an internal combustion engine, which is accepted by the public far more readily than the narrow-band, high-frequency noise spectrum of electric drives.

In a previous work [24], the basic concept of an analytical method for generating certain torque fluctuations was presented and tested with the example of a permanent magnet excited synchronous machine with surface magnets. Some assumptions were made to simplify the equations. In general, the reluctance of the rotor in the d- and q-directions can be different for permanent magnet excited synchronous machines with interior magnets (IPMSM). This makes the contributions of the reluctance torque no longer negligible. Therefore, in this publication this restriction shall be removed, and the method presented in [24] shall be extended to IPMSM.

2. Fundamentals

2.1. Machine Equations for Permanent Magnet Excited Synchronous Machines with Interior Magnets

In the following, an IPMSM in a star connection is assumed, the phases of which are shifted by 120° from each other. The following assumptions should also apply:

- The magnetic permeability, μ_{FE} , of the iron is close to infinity, so there should be almost no saturation of the iron;
- Due to the large difference, $\mu_{FE} \gg \mu_0$, it is acceptable that the field lines are perpendicular at the air-iron transition;
- Edge effects on the front side of the rotor and stator are neglected;
- The magnetic behavior of the permanent magnets is linear;
- The given equations are applied in the armature range without field weakening.

Figure 1 shows the simplified electrical equivalent circuit diagram of such a machine.

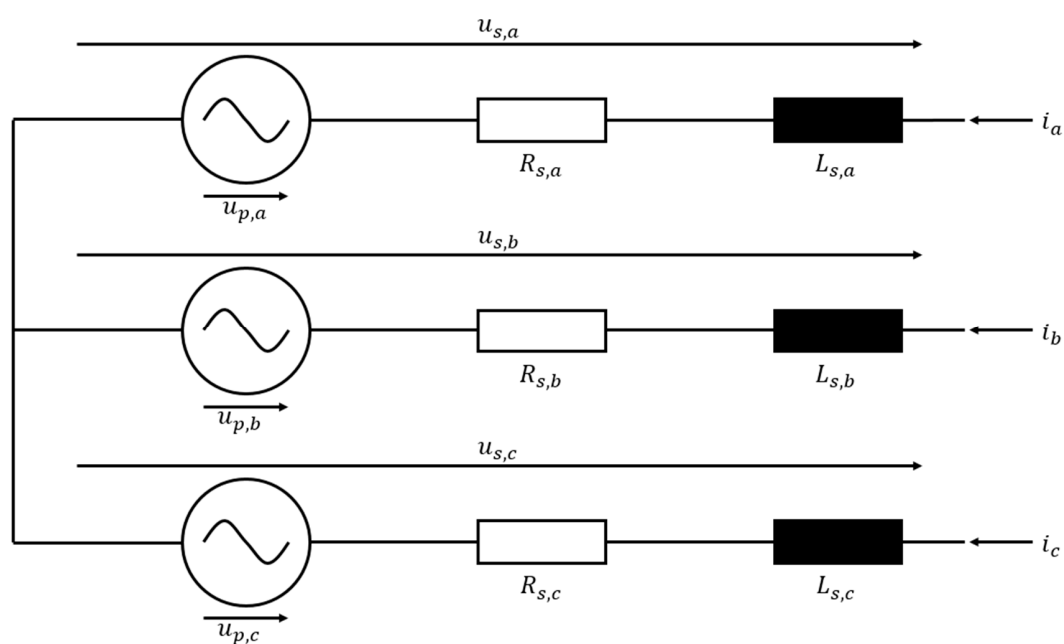


Figure 1. Simplified electrical equivalent circuit of a synchronous machine in star connection.

The machine equations can be stated as follows:

$$u_s = R_s i_s + \frac{d\psi_s}{dt} \quad (1)$$

$$\psi_s = L_s i_s + \psi'_{PM} \quad (2)$$

with u_s as the phase voltage, i_s as the phase current, R_s as the ohmic resistance in the phase, ψ_s as the stator flux, L_s as the phase inductance and ψ'_{PM} as the flux linkage of the permanent magnet to the stator windings. With Equation (3), the change in the flux linkage of the permanent magnets can be defined as back electromotive force (back-EMF), u_p .

$$u_p = \frac{d\psi'_{PM}}{dt} \quad (3)$$

Inserting Equations (2) and (3) into Equation (1) results in the equation for the phase voltage:

$$u_s = R_s i_s + L_s \frac{di_s}{dt} + u_p \quad (4)$$

A more detailed consideration of the flux linkage allows the inductances to be divided into self-inductance, L_{xx} , and mutual inductance, M_{xy} . Together with Equation (4), the phase voltages can then be represented in matrix notation:

$$\begin{pmatrix} u_a \\ u_b \\ u_c \end{pmatrix} = \begin{pmatrix} R_{s,a} & 0 & 0 \\ 0 & R_{s,b} & 0 \\ 0 & 0 & R_{s,c} \end{pmatrix} \begin{pmatrix} i_a \\ i_b \\ i_c \end{pmatrix} + \begin{pmatrix} L_{aa} & M_{ab} & M_{ac} \\ M_{ba} & L_{bb} & M_{bc} \\ M_{ca} & M_{cb} & L_{cc} \end{pmatrix} \frac{d}{dt} \begin{pmatrix} i_a \\ i_b \\ i_c \end{pmatrix} + \begin{pmatrix} u_{p,a} \\ u_{p,b} \\ u_{p,c} \end{pmatrix} \quad (5)$$

The indices a , b and c stand for the respective phase.

2.2. System of Currents

In order to operate a three-phase machine, a power supply system is required which is split into the phases i_a , i_b and i_c . In the examined scenario of a star connection without neutral conductor, the three phases have to satisfy the condition:

$$i_a + i_b + i_c = 0 \quad (6)$$

The symmetrical current system has established itself as the preferred solution in practice. This system is described in detail in the literature [25–27]. The restriction for this system is that no harmonic currents with a frequency equal to a multiple of three may be fed into the system; if this is not the case, the condition of Equation (6) is violated.

By abandoning the requirement for a symmetrical current pattern, it is possible to apply an asymmetrical current system. In this case, the fundamental waves are still symmetrically fed into the power system with a shift in phase of 120 degrees. As injected harmonics do not require an identical form in all three phases, we can feed harmonic currents with a frequency multiple of three into the system without violating the condition of Equation (6). A detailed description can be found in [24].

Equation (7) provides the combined current system in sinusoidal form:

$$\begin{aligned}
 i_a &= \sum_{j \in N_{sym}} \hat{I}_{sym,j} \sin(j\omega_e t + \gamma_{sym,j}) + \sum_{k \in N_{asym}} \hat{I}_{asym,k} \sin(k\omega_e t + \gamma_{asym,k}) \\
 i_b &= \sum_{j \in N_{sym}} \hat{I}_{sym,j} \sin(j(\omega_e t - \frac{2}{3}\pi) + \gamma_{sym,j}) \\
 &\quad + \sum_{k \in N_{asym}} \hat{I}_{asym,k} \sin(k(\omega_e t - \frac{2}{3}\pi) + \gamma_{asym,k}) \\
 i_c &= \sum_{j \in N_{sym}} \hat{I}_{sym,j} \sin(j(\omega_e t - \frac{4}{3}\pi) + \gamma_{sym,j}) \\
 &\quad + \sum_{k \in N_{asym}} \hat{I}_{asym,k} \sin(k(\omega_e t - \frac{4}{3}\pi) + \gamma_{asym,k})
 \end{aligned} \tag{7}$$

N_{sym} stands for the set of all harmonics of the symmetrical current system, and N_{asym} stands for the set of all harmonics of the asymmetrical current system. $\hat{I}_{sym,j}$ and $\hat{I}_{asym,k}$ describe the amplitude and $\gamma_{sym,j}$ and $\gamma_{asym,k}$ describe the phase-angle of the respective harmonics of the symmetrical and the asymmetrical current systems. ω_e defines the electrical frequency the current system works with.

2.3. Back Electromotive Force

Voltages are induced in the stator coils by the rotation of the permanent magnets. It is possible to measure these voltages between the neutral point and the corresponding phase in a PMSM working without a load. This voltage corresponds directly to the back-EMF, neglecting the saturation effects in iron [28].

In order to bring the analytical equations into a proper form, we approximate the shape of the voltage through a Fourier series, because the voltage is not perfectly sinusoidal. Nevertheless, many machines are designed for almost sinusoidal shapes of the back-EMF, so that the very first elements of the series are often sufficient. This leads to the following presentation for the back-EMF:

$$\begin{aligned}
 u_{p,a} &= \sum_{\mu \in N_\mu} \hat{U}_{p,\mu} \sin(\mu\omega_e t) \\
 u_{p,b} &= \sum_{\mu \in N_\mu} \hat{U}_{p,\mu} \sin(\mu(\omega_e t - \frac{2}{3}\pi)) \\
 u_{p,c} &= \sum_{\mu \in N_\mu} \hat{U}_{p,\mu} \sin(\mu(\omega_e t - \frac{4}{3}\pi))
 \end{aligned} \tag{8}$$

N_μ stands for the set of all harmonics of the back-EMF. $\hat{U}_{p,\mu}$ describes the amplitudes of the respective harmonics of the back-EMF.

2.4. Analytical Model of the Inductances

For IPMSM, the self- and mutual inductances L_{xx} and M_{xy} are functions depending on the rotor angle θ_{rot} in the rotor fixed system. They can be described by Equations (9) and (10) [28]:

$$L_{xx}(\theta_{rot}) = \int_0^{2\pi} w_x^2(\theta_s) \wp(\theta_s - \theta_{rot}) d\theta_s \tag{9}$$

$$M_{xy}(\theta_{rot}) = \int_0^{2\pi} w_x(\theta_s) w_y(\theta_s) \wp(\theta_s - \theta_{rot}) d\theta_s \tag{10}$$

with $w_x(\theta_s)$ as the winding function for phase a, b or c, $\wp(\theta_s - \theta_{rot})$ as the permeance function and θ_s as the rotor angle in the stator fixed system. Equations (9) and (10) respectively apply analogously for $L_{aa}(\theta_{rot})$, $L_{bb}(\theta_{rot})$, $L_{cc}(\theta_{rot})$, $M_{ab}(\theta_{rot})$, $M_{bc}(\theta_{rot})$ and $M_{ca}(\theta_{rot})$.

The winding function describes the number of links between the winding and the flux density. If it is a distributed winding, it corresponds to the number of windings. The general representation of the winding function is:

$$w_x(\theta_s) = \sum_n W_n \cos(n\theta_s - n\theta_x) \quad (11)$$

with θ_x as the angle of the corresponding phase—0 for phase a, $\frac{2\pi}{3}$ for phase b and $\frac{4\pi}{3}$ for phase c.

For IPMSM, the permeability function can be assumed as a trapezoidal function and approximated by Fourier series [28]:

$$\wp(\theta_{rot}) = \wp_0 + \sum_{n=Z_p}^{\infty} \wp_n \cos(n\theta_{rot}) \quad (12)$$

After some transformations, which are listed in [28], the self- and mutual inductances can be brought into the following form:

$$L_{xx} = L_0 + \sum_{n_l}^{\infty} L_{n_l} \cos(n_l(\theta_{rot} - s\frac{2\pi}{3}) + \beta_{n_l}), \quad n_l = 2, 4, 6, \dots \quad (13)$$

$$M_{xy} = M_0 + \sum_{n_m}^{\infty} M_{n_m} \cos(n_m(\theta_{rot} - s\frac{2\pi}{3} - \frac{\pi}{3}) + \beta_{n_m}), \quad n_m = 2, 4, 6, \dots \quad (14)$$

with $s = 0, 1, 2$ for the respective phase a, b or c, L_{n_l} and M_{n_m} as the amplitude, and β_{n_l} and β_{n_m} as the phase-angles of the self- and mutual inductances, respectively. L_0 and M_0 stand for their constant components.

2.5. Torque Generation

The torque in a permanent magnet excited synchronous machine, T_{em} , can be divided into three parts: the alignment torque, T_{align} , the cogging torque, T_{cog} and the reluctance torque, T_{rel} [29].

$$T_{em}(t) = T_{align}(t) + T_{rel}(t) + T_{cog}(t) \quad (15)$$

Only the alignment torque and the reluctance torque contribute to the average torque. With IPMSM, the reluctance torque cannot be neglected due to the reluctance differences of the rotor, and must be included in the calculations.

2.5.1. Alignment Torque

The alignment torque is created by the interaction of the magnetic field of the permanent magnets in the rotor with the rotating magnetic field generated by the coils in the stator. The total torque is the sum of the torques of the respective coils [29].

$$T_{align} = \frac{1}{\omega_r} \cdot (i_a u_{p,a} + i_b u_{p,b} + i_c u_{p,c}) \quad (16)$$

with ω_r representing the rotational speed of the rotor. If Equations (7) and (8) are used in Equation (16), the alignment torque can be converted into the following form (compare [24]):

$$T_{align}(t) = \frac{3}{2\omega_r} \left(\sum_{\mu \in N_\mu} \sum_{j \in N_{sym}} (\hat{I}_{sym,j} \hat{U}_{p,\mu} \sin(\gamma_{sym,j}) \sin((j \pm \mu)\omega_e t)) \right. \\ + \hat{I}_{sym,j} \hat{U}_{p,\mu} \cos(\gamma_{sym,j}) \cos((j \pm \mu)\omega_e t)) \\ + \sum_{\mu \in N_\mu} \sum_{k \in N_{asym}} (\hat{I}_{asym,k} \hat{U}_{p,\mu} \sin(\gamma_{asym,k}) \sin((k \pm \mu)\omega_e t)) \\ \left. + \hat{I}_{asym,k} \hat{U}_{p,\mu} \cos(\gamma_{asym,k}) \cos((k \pm \mu)\omega_e t)) \right) \quad (17)$$

2.5.2. Cogging Torque

In the following, we do not examine the cogging torque in detail. Although it contributes to the torque oscillations, it is only dependent on the stator shape and rotor flux. Those are generally constant for PMSM and therefore cannot be influenced by external control interventions.

2.5.3. Reluctance Torque

The Gaussian law for magnetism states that the field of magnetic flux density, B , has no sources, so the magnetic flux always forms a closed loop. The exact course of the field lines depends on the magnetic reluctance of the materials in their environment. The flux concentration in materials with low magnetic reluctance forms strong temporary poles, and causes mechanical forces oriented towards areas of higher flux.

The reluctance torque is the result of a magnetically uneven air gap in a PMSM, as the stator field attempts to align the rotor so that the magnetic reluctance of the stator flux path is minimized [28]. The reluctance torque in IPMSM can be calculated with the magnetic co-energy, W_{co} [30].

$$T_{rel} = Z_p \frac{\partial W_{co}}{\partial \theta_{rot}} \Big|_{I \text{ constant}} \quad (18)$$

with pole pair number, Z_p , and rotor angle, θ_{rot} . In a linear magnetic system, the co-energy corresponds to the energy stored in the system:

$$W_{co} = \frac{1}{2} Z_p [I(t)]^T [L(\theta)] [I(t)] \quad (19)$$

Using the current vector, $I(t)$, and the inductance matrix, $L(\theta)$, already used in Equation (5), the reluctance moment can be calculated as follows:

$$T_{rel} = Z_p \left(\frac{1}{2} i_a^2 \frac{dL_{aa}}{d\theta_{rot}} + \frac{1}{2} i_b^2 \frac{dL_{bb}}{d\theta_{rot}} + \frac{1}{2} i_c^2 \frac{dL_{cc}}{d\theta_{rot}} + i_a i_b \frac{dM_{ab}}{d\theta_{rot}} + i_b i_c \frac{dM_{bc}}{d\theta_{rot}} + i_c i_a \frac{dM_{ca}}{d\theta_{rot}} \right) \quad (20)$$

Using Equations (7), (13) and (14), Equation (20) can be transformed as follows:

$$\begin{aligned} T_{rel} = -Z_p \left(\frac{1}{2} \sum_{s=0}^2 \left[\left(\sum_{j \in N_{sym}} \hat{I}_{sym,j} \sin(j(\omega_e t - s \frac{2}{3}\pi) + \gamma_{sym,j}) \right. \right. \right. \\ \left. \left. + \sum_{k \in N_{asym}} \hat{I}_{asym,k} \sin(k\omega_e t - s \frac{2}{3}\pi + \gamma_{asym,k}) \right)^2 \right. \\ \left. \cdot \left(\sum_{n_l}^{\infty} n_l L_{n_l} \sin(n_l(\theta - s \frac{2\pi}{3}) + \beta_{n_l}) \right) \right. \\ \left. + \left(\sum_{j \in N_{sym}} \hat{I}_{sym,j} \sin(j(\omega_e t - s \frac{2}{3}\pi) + \gamma_{sym,j}) \right. \right. \\ \left. \left. + \sum_{k \in N_{asym}} \hat{I}_{asym,k} \sin(k\omega_e t - s \frac{2}{3}\pi + \gamma_{asym,k}) \right) \right. \\ \left. \cdot \left(\sum_{j \in N_{sym}} \hat{I}_{sym,j} \sin(j(\omega_e t - (s+1) \frac{2}{3}\pi) + \gamma_{sym,j}) \right. \right. \\ \left. \left. + \sum_{k \in N_{asym}} \hat{I}_{asym,k} \sin(k\omega_e t - (s+1) \frac{2}{3}\pi + \gamma_{asym,k}) \right) \right. \\ \left. \cdot \left(\sum_{n_m}^{\infty} n_m M_{n_m} \sin(n_m(\theta - s \frac{2\pi}{3} - \frac{\pi}{3}) + \beta_{n_m}) \right) \right] \Bigg) \quad (21) \end{aligned}$$

For space reasons, the terms should not be fully multiplied here, but this results in three parts for the reluctance torque—the first part is composed of the terms of the symmetrical current system,

$T_{rel, sym}$, the second part is composed of the terms of the asymmetrical current system, $T_{rel, asym}$, and the third part is composed of the combined terms of both systems, $T_{rel, comb}$:

$$T_{rel} = T_{rel, sym} + T_{rel, asym} + T_{rel, comb} \quad (22)$$

The symmetric part is used to show the structure of the equations. The multiplication results in combinations of sinusoidal terms, which generate harmonics in the torque depending on the injected harmonics in the current:

$$\begin{aligned} T_{rel, sym} &= -\frac{1}{8} Z_p \sum_{j \in N_{sym}} \hat{I}_j^2 \left(\sum_{n_l} n_l L_{n_l} \left(2 \cdot m_{j, n_l}^{+-} - m_{j, n_l}^{++} - m_{j, n_l}^{--} \right) \right. \\ &\quad \left. + \sum_{n_m} n_m M_{n_m} \left(2 \cdot m_{j, n_m}^{+-} - m_{j, n_m}^{++} - m_{j, n_m}^{--} \right) \right) \\ m_{j, n_l}^{+-} &= \sum_{s=0}^2 \sin \left(n_l \left(\omega_e t - s \frac{2}{3} \pi \right) + \beta_{n_l} \right) \\ m_{j, n_l}^{++} &= \sum_{s=0}^2 \sin \left((n_l + 2 \cdot j) \left(\omega_e t - s \frac{2}{3} \pi \right) + 2 \cdot \gamma_{sym, j} + \beta_{n_l} \right) \\ m_{j, n_l}^{--} &= \sum_{s=0}^2 \sin \left((n_l - 2 \cdot j) \left(\omega_e t - s \frac{2}{3} \pi \right) - 2 \cdot \gamma_{sym, j} + \beta_{n_l} \right) \\ m_{j, n_m}^{+-} &= \sum_{s=0}^2 \sin \left(n_m \left(\omega_e t - s \frac{2}{3} \pi \right) + j \frac{2\pi}{3} - n_m \frac{\pi}{3} + \beta_{n_m} \right) \\ m_{j, n_m}^{++} &= \sum_{s=0}^2 \sin \left((n_m + 2 \cdot j) \left(\omega_e t - s \frac{2}{3} \pi \right) - j \frac{2\pi}{3} - n_m \frac{\pi}{3} + 2 \cdot \gamma_{sym, j} + \beta_{n_m} \right) \\ m_{j, n_m}^{--} &= \sum_{s=0}^2 \sin \left((n_m - 2 \cdot j) \left(\omega_e t - s \frac{2}{3} \pi \right) + j \frac{2\pi}{3} - n_m \frac{\pi}{3} - 2 \cdot \gamma_{sym, j} + \beta_{n_m} \right) \end{aligned} \quad (23)$$

3. Approach

The approach presented in [24] shall now be extended for IPMSM by the reluctance torque. Equation (15) is transformed for this purpose:

$$T_{align}(t) + T_{rel}(t) = T_{em}(t) - T_{cog}(t) \quad (24)$$

The desired nominal torque is approximated by Equation (25), and the cogging torque is divided in a similar way by a Fourier series (see Equation (26)).

$$T_{em}(t) = T_{nom}(t) = \sum_{l \in N_{nom}} \hat{T}_{nom, l} \cdot \cos(\gamma_{nom, l}) \cdot \sin(l \omega_e t) + \hat{T}_{nom, l} \cdot \sin(\gamma_{nom, l}) \cdot \cos(l \omega_e t) \quad (25)$$

$$T_{cog}(t) = \sum_{g \in N_{cog}} \hat{T}_{cog, g} \cdot \cos(\gamma_{cog, g}) \cdot \sin(g \omega_e t) + \hat{T}_{cog, g} \cdot \sin(\gamma_{cog, g}) \cdot \cos(g \omega_e t) \quad (26)$$

with $\hat{T}_{nom, l}$ and $\hat{T}_{cog, g}$ as amplitudes and $\gamma_{nom, l}$ and $\gamma_{cog, g}$ as phase-angles of the nominal and cogging torque. N_{nom} and N_{cog} stand for the set of all the harmonics of both torques.

If Equations (17), (21), (25) and (26) are now set into Equation (24), this can be represented as a linear combination of the independent basis vectors $\sin(n \omega_e t)$ and $\cos(n \omega_e t) \mid n \in N_{nom} \cup N_{cog}$, where N_{nom} and N_{cog} are the set of all harmonics of the desired torque, as well as the cogging torque. A coefficient comparison between both sides of the equation yields a system of equations with $2n$ equations of the following form (compare [24]):

$$\mathbf{U} \cdot \underline{x} = \underline{h} \quad (27)$$

4. Validation

4.1. Machine Parameters

First of all, the analytical calculation method of the reluctance torque is to be validated. For this purpose, a three-phase, star-connected IPMSM with parameters listed in Table 1 was set up in Ansys Maxwell. Figure 2 shows the arrangement of the permanent magnets in the rotor and Table 2 contains the corresponding characteristic values of the magnets used.

Table 1. Machine parameters for validation of the analytical calculation of reluctance torque for permanent magnet excited synchronous machines with interior magnets (IPMSM).

Rated Output Power	20 kW	Number of Slots	12
Rated Voltage	320 V	Number of Conductors per Slot	58
Rated Speed	3400 rpm	Outer Diameter of Rotor	210 mm
Number of Poles	8	Length of Rotor Core	75 mm
Outer Diameter of Stator	300 mm	Length of Stator Core	75 mm
Inner Diameter of Stator	217 mm		

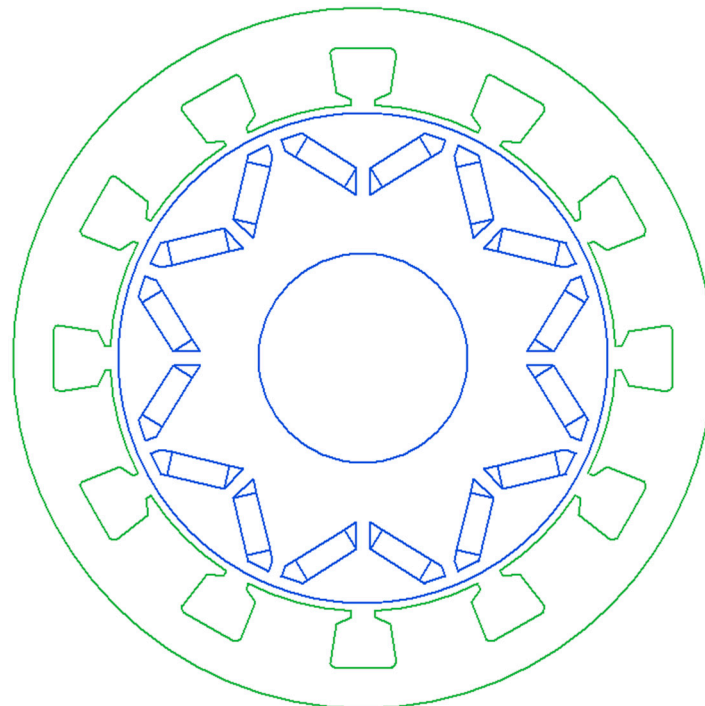


Figure 2. Cross-section through the IPMSM with magnets in V-arrangement used in the validation of the analytical method for calculating the reluctance torque.

Table 2. Magnetic parameters to validate the analytical calculation of reluctance torque for IPMSM.

Residual Flux Density	1.40 T
Coercive Force	1115 kA/m
Maximum Energy Density	390.57 kJ/m ³
Relative Recoil Permeability	1.00
Demagnetized Flux Density	0 T
Recoil Residual Flux Density	1.40 T
Recoil Coercive Force	1115 kA/m

4.2. Validation of the Torque Calculation Method for Permanent Magnet Excited Synchronous Machines with Interior Magnets

For validation in the entire armature range, 60 operating points were calculated by both finite element method (FEM) analysis and analytical methods. The operating points are composed of the parameter combinations from Table 3.

Table 3. Parameter combination possibilities of the examined operating points for validation of the analytical calculation method of the reluctance torque for IPMSM.

Current amplitude I_1	{25 A, 30 A, 35 A, 40 A, 45 A}
Stator field frequency f_e	{100 Hz, 150 Hz, 200 Hz, 250 Hz}
Phase shift of fundamental wave γ_1	{0 rad, 0.5 rad 1 rad}

To evaluate the validity of the analytical calculation method, the time course of the torque is analyzed for each of the 60 operating points by applying a Fourier transformation and calculating the resulting deviations as key indicators, e_{fund} and e_{harm} , from the amplitudes:

$$e_{fund} = \frac{T_{analytic,0} - T_{FEM,0}}{T_{FEM,0}} \cdot 100\% \quad (28)$$

$$e_{harm} = \sum_{i=1}^N \frac{|T_{analytic,i} - T_{FEM,i}|}{\sum_i^N T_{FEM,i}} \cdot 100\% \quad (29)$$

where $T_{analytic,0}$ stands for the value of the constant torque determined by the analytical calculation, $T_{FEM,0}$ corresponds to the value of the constant torque calculated by the FEM simulation, $T_{analytic,i}$ stands for the amplitude of the i th harmonic in the torque, determined by the analytical calculation, and $T_{FEM,i}$ corresponds to the amplitude of the i th harmonic in the torque calculated by FEM simulation.

Figures 3 and 4 show the distributions of the indicators for all 60 operating points, divided into the individual parameters. In the Box and Whisker Plots, there is one parameter held constant, and we show the variation in the key indicators e_{fund} and e_{harm} by varying all the other parameters.

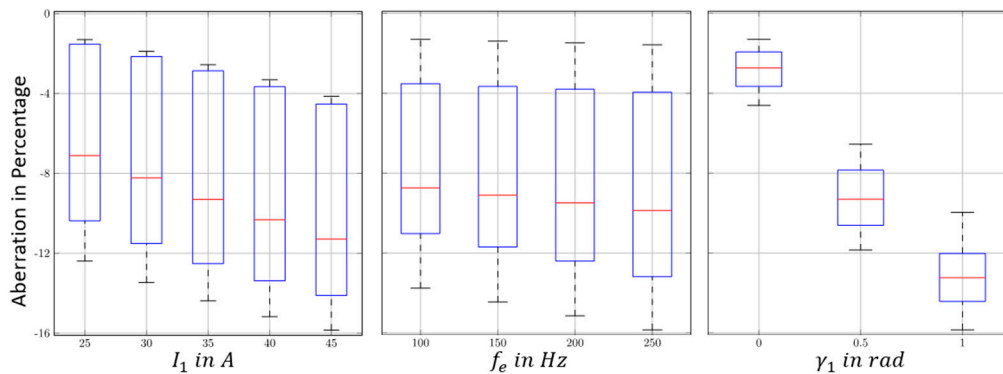


Figure 3. Distribution of the key indicator, e_{fund} for the constant torque value.

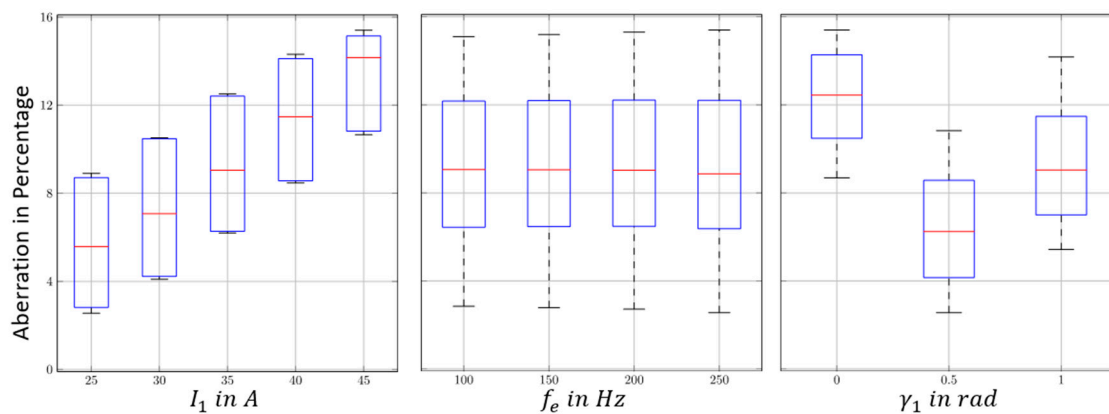


Figure 4. Distribution of the key indicator, e_{harm} for the value of harmonics in torque.

For both e_{fund} and e_{harm} , the results show a dependence on the injected current level, I_1 . For the constant value, the analytical calculation deviates in the negative direction from the FEM simulations, and for the harmonics it deviates in a positive direction. There is hardly any influence on the results from the variation in the frequency. However, the values show a wide scattering. For the change of the phase angle, the results show a strong variation. The scattering of the other parameters, when the phase angle is fixed, is, however, small.

The deviations in the key indicators lie between 1% and 16%. The closer examination of a single operating point should show the convenience of the key indicator for the analytical calculation of the torque with reluctance torque for IPMSM, compared to an analytical calculation without reluctance torque.

Figure 5 shows the time course of the torque for the operating point $I_1 = 40\text{ A}$, $f_e = 200\text{ Hz}$, $\gamma_1 = 0.5\text{ rad}$ from the FEM calculation, as well as the analytical calculation of the torque from Equation (15), once with T_{rel} and once without. Figure 6 shows the corresponding spectrum of the torques. The deviation between the constant torque is reduced from 13.7% to 5.3% by including the reluctance torque at the present operating point. The deviation in the amplitude of the sixth harmonic of the torque, which is the most dominant vibration in this machine, is reduced from 22.4% to 3.8%.

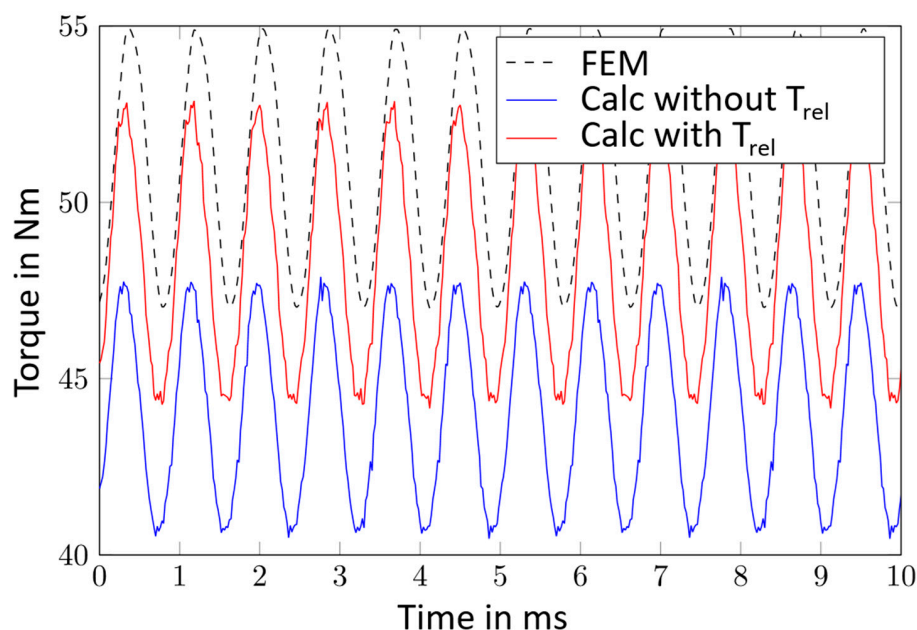


Figure 5. Time course of the torque for a selected operating point, resulting from the FEM calculation as well as from the analytical calculation with and without reluctance torque.

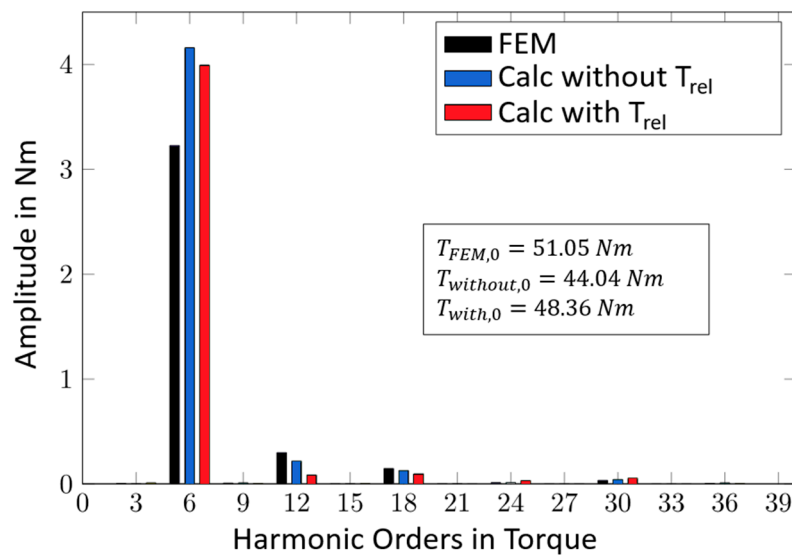


Figure 6. Order spectra of the time courses from Figure 5. For better representation, the bars for the zeroth order have been hidden and indicated by their numerical values.

4.3. Validation of Generative Harmonic Current Injection for Permanent Magnet Excited Synchronous Machines with Interior Magnets

The machine presented in Section 4.1 was also used to validate the method from Section 3, by generating a determined torque ripple via an analytical calculation, including the reluctance torque. Five scenarios were examined for validation. The required amplitudes and phase shifts of the individual scenarios are listed in Table 4. In this case, S0 corresponds to the pure suppression of torque fluctuations, which is the requirement for harmonic current injection known from the literature. The deviation of the generated harmonics in torque from the required values is also listed in Table 4, in percent.

Table 4. Requirements of the scenarios used for validation, as well as the deviation of the generated harmonics from the required values. The index value of amplitude and phase indicates the number of the required harmonic order.

Scenario	Amplitude	Phase	Deviation
S0	$\hat{T}_{nom,l} = 0$	$\gamma_{nom,j} = 0$	-
S1	$\hat{T}_{nom,1} = 5 \text{ Nm}$	$\gamma_{nom,1} = 0$	8.25%
S2	$\hat{T}_{nom,2} = 4 \text{ Nm}$	$\gamma_{nom,2} = 0.5$	6.56%
S3	$\hat{T}_{nom,9} = 4 \text{ Nm}$	$\gamma_{nom,9} = 0.9$	7.49%
S4	$\hat{T}_{nom,5} = 5 \text{ Nm}$	$\gamma_{nom,5} = 0$	8.36%
	$\hat{T}_{nom,9} = 3 \text{ Nm}$	$\gamma_{nom,9} = 0$	8.90%

For scenario S0, the calculation of percentage deviation is not appropriate, but the torque fluctuations of the dominant sixth harmonic could be reduced by 87%, from 4.02 Nm to less than 0.5 Nm. In all scenarios (including scenario S0), the constant torque was changed by a negligible 0.38% at most by injecting the additional harmonics.

In the following, scenarios S1 and S4 will be examined in more detail. Figures 7 and 8 show the respective order spectra. The value of the constant torque has been added as a numerical value for reasons of visibility.

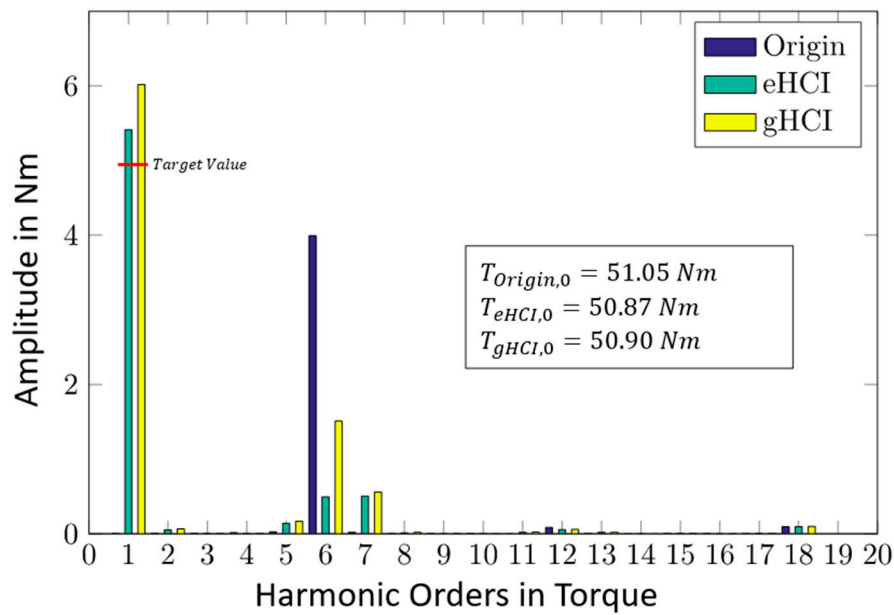


Figure 7. Order spectrum for scenario S1. For better readability, the bars for the zeroth order have been hidden and indicated by their numerical values. Extended harmonic current injection (eHCI) corresponds to the method from Section 3. Generative harmonic current injection (gHCI) corresponds to the approach from [24].

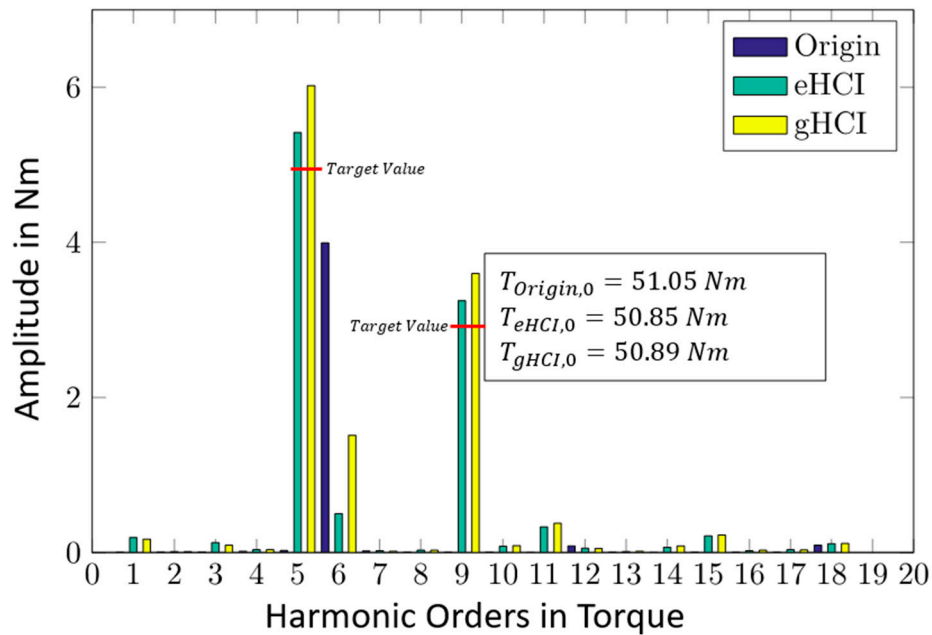


Figure 8. Order spectrum for scenario S4. For better readability, the bars for the zeroth order have been hidden and indicated by their numerical values. Extended harmonic current injection (eHCI) corresponds to the method from Section 3. Generative harmonic current injection (gHCI) corresponds to the approach from [24].

For scenario S1, the method presented in this paper provides an amplitude for the first harmonic in the torque of 5.40 Nm, which is thus 13.0% closer to the required value than the approach from [24]. In addition, parasitic harmonics, such as the fifth, sixth and seventh harmonics, result in lower amplitudes (see Figure 7).

The same applies to Scenario S4. The required fluctuations are generated with 5.42 Nm for the fifth harmonic and with 3.27 Nm for the ninth harmonic, with 12.6% and 11.8% more accuracy than the method without reluctance torque. The parasitic harmonics are also at a lower level (see Figure 8).

5. Conclusions

Figures 3 and 4 show that the operating point examined in more detail in Section 4.2 is one of the parameter combinations with the greatest deviations in the examination area. The results show, by calculating the torque with inclusion of the reluctance torque, that there is still a deviation from the FEM calculation, but it is a significant improvement over the analytical method from [24] without the reluctance torque. The differences between the FEM calculation and the presented analytical method with reluctance torque, which can still be seen for example in Figure 6, can partly be attributed to the neglect of loss and saturation effects in the analytical equations.

The saturation effects in iron reduce the amplitudes of the harmonics by several percent. In real machines, it is therefore quite possible that somewhat stronger currents have to be injected than the method predicts in order to achieve the same effect. There are also disadvantages in the area of higher harmonic orders, but in the dominant area of the constant torque and the sixth harmonic the analytical calculation with reluctance torque is better.

In general, it can be said that the results from the analytical calculation correspond well with those from the FEM simulation. Therefore, the equations from Section 2 for calculating the torque for synchronous machines with buried permanent magnets are definitely applicable.

The deviations of the torque variation from the desired torque variation in Table 4 are below 9% in all scenarios. The currents calculated beforehand by the analytical method, which are injected into the synchronous machine, thus deliver the desired torque with sufficient accuracy.

A closer look at the results from Section 4.3 shows that the amplitudes of the desired orders are slightly above the required values. This was the case for all scenarios. Nevertheless, the results are on average 12% closer to the required value than the variant without reluctance torque. In addition, the oscillation of the sixth harmonic in the torque, which should become zero for both scenario 1 and scenario 4, can be compensated much better. Further, parasitic harmonics have a lower amplitude than that achieved with the method from [24].

The results thus show that the extension of the method from [24] using the reluctance torque for IPMSM provides significantly more accurate results. They also show the general applicability of the method from Section 3 to obtain the specifically desired torque ripples.

6. Summary

In the present work, an analytical method for generating certain torque fluctuations in permanent magnet excited synchronous machines with surface magnets was extended in such a way that it is also valid for synchronous machines with embedded magnets. This was achieved by including the reluctance torque in the equations.

First, the analytical equations for the machine and the current system were derived. The asymmetric current system, which is used to generate harmonics that do not correspond to a multiple of three, was briefly discussed again. After deriving the analytical equations for the inductances in the machine, the individual elements of the torque were explained. Special attention was given to the equations of reluctance torque, which is no longer negligible for synchronous machines with embedded magnets.

Next, the approach to solving the equations was briefly described. This provided the amplitudes and phases of the harmonics in the currents that are necessary to generate the required amplitudes in the torque. Furthermore, the derivation of the reluctance torque was validated by means of FEM simulations, and was then compared with the results from the calculation of [24]. It was shown that for synchronous machines with embedded magnets, the calculation of the torque according to the equations of this publication gives significantly better results.

Finally, the method was validated in several fictional scenarios by further FEM simulations. It was shown that the required fluctuations can be generated with small deviations, and the method is significantly more accurate for synchronous machines with embedded magnets than the method in [24].

Author Contributions: Conceptualization, M.V.; methodology, M.V.; software, J.L.; validation, J.L.; formal analysis, M.V. and J.L.; resources, F.G.; data curation, J.L.; writing—original draft preparation, M.V.; writing—review and editing, J.L. and F.G.; visualization, M.V.; supervision, F.G.; project administration, M.V. and F.G. All authors have read and agreed to the published version of the manuscript.

Funding: This research received no external funding

Acknowledgments: We acknowledge support by the KIT-Publication Fund of the Karlsruhe Institute of Technology.

Conflicts of Interest: The authors declare no conflict of interest.

References

1. Zeraoulia, M.; Benbouzid, M.E.H.; Diallo, D. Electric Motor Drive Selection Issues for HEV Propulsion Systems: A Comparative Study. *IEEE Trans. Veh. Technol.* **2006**, *55*, 1756–1764. [\[CrossRef\]](#)
2. Kangkang, Z.; Jianqiu, L.; Minggao, O.; Jing, G.; Yan, M. Electric braking performance analysis of PMSM for electric vehicle applications. In Proceedings of the 2011 International Conference on Electronic & Mechanical Engineering and Information Technology, Harbin, China, 12–14 August 2011; pp. 2596–2599.
3. Li, Y.; Gerling, D.; Ma, J.; Liu, J.; Yu, Q. The Comparison of Control Strategies for the Interior PMSM Drive Used in the Electric Vehicle. *World Electr. Veh. J.* **2010**, *4*, 648–654. [\[CrossRef\]](#)
4. Kimura, T.; Saitou, R.; Kubo, K.; Nakatsu, K.; Ishikawa, H.; Sasaki, K. High-power-density inverter technology for hybrid and electric vehicle applications. *Hitachi Rev.* **2014**, *63*, 42–47.
5. Levi, E. Advances in Converter Control and Innovative Exploitation of Additional Degrees of Freedom for Multiphase Machines. *IEEE Trans. Ind. Electron.* **2016**, *63*, 433–448. [\[CrossRef\]](#)
6. Holtz, J.; Springob, L. Identification and compensation of torque ripple in high-precision permanent magnet motor drives. *IEEE Trans. Ind. Electron.* **1996**, *43*, 309–320. [\[CrossRef\]](#)
7. Magnussen, F.; Thelin, P.; Sadarangani, C. Performance evaluation of permanent magnet synchronous machines with concentrated and distributed windings including the effect of field-weakening. In Proceedings of the Second International Conference on Power Electronics, Machines and Drives (PEMD 2004), Edinburgh, UK, 31 March–2 April 2004; p. v2-679.
8. Han, S.-H.; Jahns, T.M.; Soong, W.L. Torque Ripple Reduction in Interior Permanent Magnet Synchronous Machines Using the Principle of Mutual Harmonics Exclusion. In Proceedings of the 2007 IEEE Industry Applications Annual Meeting, New Orleans, LA, USA, 23–27 September 2007; pp. 558–565.
9. Han, S.-H.; Jahns, T.M.; Soong, W.L.; Guven, M.K.; Illindala, M.S. Torque Ripple Reduction in Interior Permanent Magnet Synchronous Machines Using Stators with Odd Number of Slots Per Pole Pair. *IEEE Trans. Energy Convers.* **2010**, *25*, 118–127. [\[CrossRef\]](#)
10. Bianchi, N.; Bolognani, S.; Pre, M.D.; Grezzani, G. Design considerations for fractional-slot winding configurations of synchronous machines. *IEEE Trans. Ind. Appl.* **2006**, *42*, 997–1006. [\[CrossRef\]](#)
11. Chung, D.-W.; You, Y.-M. Cogging Torque Reduction in Permanent-Magnet Brushless Generators for Small Wind Turbines. *J. Magn.* **2015**, *20*, 176–185. [\[CrossRef\]](#)
12. Kwack, J.; Min, S.; Hong, J.-P. Optimal Stator Design of Interior Permanent Magnet Motor to Reduce Torque Ripple Using the Level Set Method. *IEEE Trans. Magn.* **2010**, *46*, 2108–2111. [\[CrossRef\]](#)
13. Kim, K.-C. A Novel Method for Minimization of Cogging Torque and Torque Ripple for Interior Permanent Magnet Synchronous Motor. *IEEE Trans. Magn.* **2014**, *50*, 793–796. [\[CrossRef\]](#)
14. Ren, W.; Xu, Q.; Li, Q. Asymmetrical V-Shape Rotor Configuration of an Interior Permanent Magnet Machine for Improving Torque Characteristics. *IEEE Trans. Magn.* **2015**, *51*, 1–4. [\[CrossRef\]](#)
15. Dajaku, G.; Gerling, D. New methods for reducing the cogging torque and torque ripples of PMSM. In Proceedings of the 4th International Electric Drives Production Conference (EDPC), Nuremberg, Germany, 30 September–1 October 2014; pp. 1–7.
16. Hwang, M.-H.; Lee, H.-S.; Cha, H.-R. Analysis of Torque Ripple and Cogging Torque Reduction in Electric Vehicle Traction Platform Applying Rotor Notched Design. *Energies* **2018**, *11*, 3053. [\[CrossRef\]](#)

17. Islam, M.S.; Islam, R.; Sebastian, T. Experimental Verification of Design Techniques of Permanent-Magnet Synchronous Motors for Low-Torque-Ripple Applications. *IEEE Trans. Ind. Appl.* **2011**, *47*, 88–95. [[CrossRef](#)]
18. Petrov, I.; Ponomarev, P.; Alexandrova, Y.; Pyrhonen, J. Unequal Teeth Widths for Torque Ripple Reduction in Permanent Magnet Synchronous Machines with Fractional-Slot Non-Overlapping Windings. *IEEE Trans. Magn.* **2015**, *51*, 1–9. [[CrossRef](#)]
19. Favre, E.; Cardoletti, L.; Jufer, M. Permanent-magnet synchronous motors: A comprehensive approach to cogging torque suppression. *IEEE Trans. Ind. Appl.* **1993**, *29*, 1141–1149. [[CrossRef](#)]
20. Najmabadi, A.; Xu, W.; Degner, M. A Sensitivity Analysis on the Fifth and the Seventh Harmonic Current Injection for Sixth Order Torque Ripple Reduction. In Proceedings of the IEEE International Electric Machines and Drives Conference (IEMDC), Miami, FL, USA, 21–24 May 2017.
21. Zhu, Z.Q.; Wu, L.J.; Xia, Z.P. An Accurate Subdomain Model for Magnetic Field Computation in Slotted Surface-Mounted Permanent-Magnet Machines. *IEEE Trans. Magn.* **2010**, *46*, 1100–1115. [[CrossRef](#)]
22. Baodong, C.; Gang, L.; Kun, M. Harmonic current suppression for high-speed permanent magnet synchronous motor with sensorless control. In Proceedings of the 19th International Conference on Electrical Machines and Systems (ICEMS), Chiba, Japan, 13–16 November 2016.
23. Feng, G.; Lai, C.; Kar, N.C. Practical Testing Solutions to Optimal Stator Harmonic Current Design for PMSM Torque Ripple Minimization Using Speed Harmonics. *IEEE Trans. Power Electron.* **2018**, *33*, 5181–5191. [[CrossRef](#)]
24. Vollat, M.; Hartmann, D.; Gauterin, F. An Analytical Method for Generating Determined Torque Ripple in Synchronous Machines with Surface Magnets by Harmonic Current Injection. *Machines* **2020**, *8*, 32. [[CrossRef](#)]
25. Hanselman, D. *Brushless Permanent Magnet Motor Design*; Magna Physics Pub: Lebanon, OH, USA, 2006.
26. Krause, P.C.; Wasynczuk, O.; Sudhoff, S.D.; Pekarek, S. *Analysis of Electric Machinery and Drive Systems*, 3rd ed.; Wiley IEEE Press: Hoboken, NJ, USA, 2013.
27. Schröder, D. *Elektrische Antriebe—Regelung von Antriebssystemen, Version 4*; Springer: Berlin/Heidelberg, Germany, 2015.
28. Farshadnia, M. *Advanced Theory of Fractional-Slot Concentrated-Wound Permanent Magnet Synchronous Machines*; Springer: Singapore, 2018.
29. Hung, J.Y.; Ding, Z. Design of currents to reduce torque ripple in brushless permanent magnet motors. *IEEE Proc. B Electr. Power Appl. UK* **1993**, *140*, 260. [[CrossRef](#)]
30. Hamiti, T.; Lubin, T.; Baghli, L.; Rezzoug, A. Modeling of a synchronous reluctance machine accounting for space harmonics in view of torque ripple minimization. *Math. Comput. Simul.* **2010**, *81*, 354–366. [[CrossRef](#)]

Publisher’s Note: MDPI stays neutral with regard to jurisdictional claims in published maps and institutional affiliations.



© 2020 by the authors. Licensee MDPI, Basel, Switzerland. This article is an open access article distributed under the terms and conditions of the Creative Commons Attribution (CC BY) license (<http://creativecommons.org/licenses/by/4.0/>).